Biophysical Chemistry 158 (2011) 26–37

Contents lists available at ScienceDirect

Biophysical Chemistry

journal homepage: http://www.elsevier.com/locate/biophyschem

Interactions of the DNA polymerase X from African Swine Fever Virus with the ssDNA. Properties of the total DNA-binding site and the strong DNA-binding subsite ☆

Maria J. Jezewska, Michal R. Szymanski, Wlodzimierz Bujalowski *

Department of Biochemistry and Molecular Biology, The University of Texas Medical Branch at Galveston, 301 University Boulevard, Galveston, Texas 77555–1053, United States
Department of Obstetrics and Gynecology, The University of Texas Medical Branch at Galveston, 301 University Boulevard, Galveston, Texas 77555–1053, United States
The Sealy Center for Structural Biology, Sealy Center for Cancer Cell Biology, The University of Texas Medical Branch at Galveston, 301 University Boulevard, Galveston, Texas 77555–1053, United States

ARTICLE INFO

Article history:
Received 16 March 2011
Received in revised form 8 April 2011
Accepted 18 April 2011
Available online 28 April 2011

Keywords:
Polymerase
DNA replication
Protein–DNA interaction
Motor protein
Fluorescence titrations

ABSTRACT

Interactions of the polymerase X from the African Swine Fever Virus with the ssDNA have been studied, using quantitative fluorescence titration and fluorescence resonance energy transfer techniques. The primary DNA-binding subsite of the enzyme, independent of the DNA conformation, is located on the C-terminal domain. Association of the bound DNA with the catalytic N-terminal domain finalizes the engagement of the total DNA-binding site of the enzyme and induces a large topological change in the structure of the bound ssDNA. The free energy of binding includes a conformational transition of the protein. Large positive enthalpy changes accompanying the ASFV pol X–ssDNA association indicate that conformational changes of the complex are induced by the engagement of the N-terminal domain. The enthalpy changes are offset by large entropy changes accompanying the DNA binding to the C-terminal domain and the total DNA-binding site, predominantly resulting from the release of water molecules.

1. Introduction

The African Swine Fever Virus (ASFV) has been the subject of intensive studies as the etiological agent responsible for acute hemorrhagic fever in domestic pigs [1–5]. The ASFV polymerase X is one of the proteins coded by the virus genome, which shows significant functional similarities to DNA-repair polymerases that include distributive DNA synthesis on template-primer DNA substrates and efficient filling of single nucleotide gaps [4–6]. These functional activities and the fact that the ASFV genome codes for the replicative polymerase and several enzymes involved in the base excision repair (BER) pathway, indicate that the major role of the ASFV pol X is to repair the viral DNA damaged by the host reaction to the viral infection [4,5].

The ASFV pol X is currently the smallest known DNA polymerase with a molecular weight of ~20,000, whose structure has been determined by the NMR method [7,8]. The enzyme is built of two domains, the N-terminal domain, which includes the first 105 amino acids from the N-terminus of the protein and the C-terminal domain, comprising the remaining 69 amino acid residues, as depicted in Fig. 1a. The active site of the DNA synthesis with the triad of invariant aspartate residues is located in the N-terminal domain (Fig. 1b). Moreover, the N-terminal domain contains a positively charged helix, αC. Similarly, the C-terminal domain contains a highly positively charged helix, αE (Fig. 1a) [7,8]. Both helices were implicated in the enzyme interactions with the DNA[7,8,11]. The simplified structure of the ASFV pol X makes the enzyme an excellent model system for the examination of the properties of a DNA repair polymerase.

Quantitative thermodynamic studies provided the first indication of the intricate interactions of the ASFV pol X with the ssDNA, in spite of the simplified structure of the protein [9–11]. The total site-size of the enzyme–ssDNA complex, *i.e.*, the maximum number of nucleotides occluded by the polymerase, is 16 ± 1 nucleotides. The total DNA-binding site has a heterogeneous structure, containing the strong ssDNA-binding subsite, which encompasses only 7 ± 1 nucleotides. Moreover, the subsite shows a significant preference for the dsDNA conformation over the ssDNA [10]. Fluorescence resonance energy transfer (FRET) data showed that the dsDNA binds to the C-terminal domain of the enzyme, a strong indication that the strong ssDNA-binding subsite is located on the domain (Fig. 1a and b) [10]. The enzyme engages the weak DNA-binding subsite in interactions only with the longer ssDNA oligomers. However, the efficiency of this engagement depends on the length of the ssDNA [9].

Although significant progress has been achieved in elucidating the ASFV pol X - DNA interactions, the nature of these interactions is still

Abbreviations: ASFV, African Swine Fever Virus; DTT, dithiothreitol; ssDNA, single-stranded DNA; dsDNA, double-stranded DNA; εA, etheno-adenosine; CP, 7-Diethylamino-3-(4′-maleimidylphenyl)-4-methylcoumarin; MCT method, Macromolecular Competition Titration Method; BER, base excision repair; FRET, fluorescence resonance energy transfer.

☆ This work was supported by NIH Grants GM-58565 (to W. B.).

* Corresponding author at: Department of Biochemistry and Molecular Biology, The University of Texas Medical Branch at Galveston, 301 University Boulevard, Galveston, Texas 77555–1053, United States. Tel.: +1 409 772 5634; fax: +1 409 772 1790.
E-mail address: wbujalow@utmb.edu (W. Bujalowski).

0301-4622/$ – see front matter © 2011 Elsevier B.V. All rights reserved.
doi:10.1016/j.bpc.2011.04.012

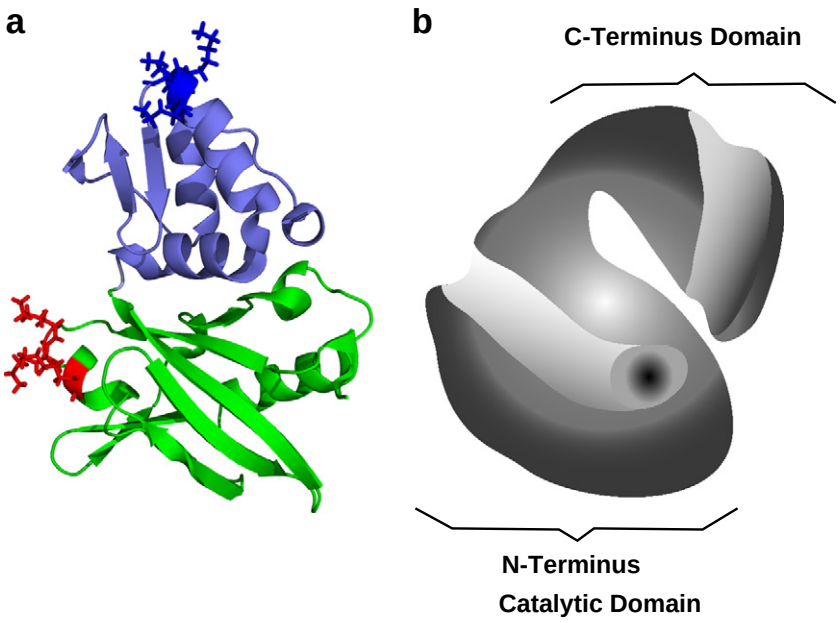

Fig. 1. a. Three-dimensional structure of the ASFV pol X obtained by NMR analyses [7,8]. The first 105 amino acid residues from the N-terminus of the protein (green) constitute the palm domain of the enzyme, while the remaining 69 amino acid residues (red) form the C-terminal domain. The lysine residues, 59, 60, and 63 contained in the αC helix of the palm domain and the lysine residues 131, 132, and 133 in the αE helix in the C-terminal domain, are marked in red and blue colors, respectively. b. Schematic representation of the ASFV pol X with the marked the strong DNA-binding subsite on the C-terminal and the weak DNA-binding subsite on the N-terminal domain, respectively. Both subsites form the total DNA-binding site of the enzyme [9,10]. The dark oval represents the location of the active site of the polymerase.

not completely understood. For instance, both the N-terminal and the C-terminal domains contain similar positively charged helices (Fig. 1a). Yet, the affinity of the strong DNA-binding subsite on the C-terminal domain is orders of magnitude higher than the affinity of the weak subsite [9–11]. Moreover, the reason for the significantly higher dsDNA-affinity of the strong subsite, as compared to its ssDNA-affinity, is unknown [10]. The NMR structure of the enzyme does not provide any clue about these different functional behaviors. While the release of only ~1 ion accompanies the exclusive ssDNA binding to the strong subsite, the release of ~6 ions occurs upon the engagement of the total DNA-binding site. These data would suggest that ionic interactions dominate the association with the weak subsite, but not the binding to the strong subsite on the C-terminal domain, though both subsites have the same number of exposed lysine residues in the presumed binding areas [7,8]. Furthermore, the structure of the DNA, exclusively bound to the strong subsite on the C-terminal domain, is characterized by a significantly larger separation and immobilization of the bound DNA bases than the structure of the bound longer DNAs, which encompass the total DNA-binding site of the polymerase.

Interactions of a DNA polymerase with the nucleic acid play a fundamental role in the functioning of the enzyme, including fidelity of the DNA synthesis, as the polymerase complex with the DNA constitutes the binding and recognition site for dNTPs [12–14]. Moreover, in the case of a DNA repair polymerase, elucidation of the enzyme - DNA interactions is of paramount importance for understanding the recognition mechanism of the damaged DNA [7–14]. In this communication, we examine the energetics of interactions of the total DNA-binding site and the strong DNA-binding subsite of the ASFV pol X with the ssDNA. The intrinsic affinity of the total site is not a simple sum of contributions from the strong and weak DNA-binding subsites. The protein–ssDNA complex undergoes a conformational transition induced by the nucleic acid interactions with the N-terminal domain. The intrinsic affinities of the strong subsite and the total DNA-binding site are predominantly driven by large entropy changes resulting from the release of water molecules from both the strong and weak DNA-binding subsites of the protein.

2. Materials and methods

2.1. Reagents and buffers

All chemicals were reagent grade. All solutions were made with distilled and deionized >18 MΩ (Milli-Q Plus) water. Standard buffer C is 10 mM sodium cacodylate adjusted to pH 7.0 with HCl, 50 mM NaCl, 1 mM $MgCl_2$, 1 mM DTT, and 10% glycerol (w/v).

2.2. The ASFV pol X

The plasmid harboring the gene of the ASFV pol X was a generous gift of Dr. Maria L. Salas (Universidad Autonoma, Madrid, Spain). Isolation and purification of the protein was performed, with slight modifications, as described [8–11]. The concentration of the protein was spectrophotometrically determined using the extinction coefficient $\varepsilon_{280} = 1.656 \times 10^5\ cm^{-1}\ M^{-1}$, obtained with the approach based on Edelhoch's method [15,16].

2.3. Nucleic acids

All unmodified and modified ssDNA oligomers were purchased from Midland Certified Reagents (Midland, Texas). The labeled ssDNA oligomer, $dT(pT)_{19}$, contains a fluorescent marker, fluorescein (Fl), attached at the 5′ end through phosphoramidate chemistry, and/or the coumarin derivative (CP), attached through the 6-carbon linker at the 3′ end. The labeled ssDNA oligomers are referred to as: 5′-Fl-$dT(pT)_{19}$, $dT(pT)_{19}$-CP-3′, and 5′-Fl-$dT(pT)_{19}$-CP-3′. The etheno-derivatives of homo-adenosine oligomers were obtained by modification with chloroacetaldehyde as previously described by us [17–23]. Concentrations of all ssDNA oligomers and the degree of labeling with the fluorescent markers, γ, have been spectrophotometrically determined [17–21,24]. The labeling with coumarin and fluorescein markers was complete in all examined oligomers and characterized by $\gamma = 1 \pm 0.03$. The dsDNA 10-mer has been built of the oligomer, ACGAGCCTGC, and the complementary strand. The integrity of the dsDNA oligomers has

been checked by UV melting and analytical ultracentrifugation techniques. In the studied solution conditions, the melting temperature of the examined dsDNA oligomer is ~54 °C (data not shown).

2.4. Fluorescence measurements

Steady-state fluorescence titrations were performed using the SLM-AMINCO 8100 C spectrofluorometer, as previously described by us [9–11,25–27]. The ASFV pol X binding was followed by monitoring the fluorescence of the etheno-derivatives of the nucleic acid ($\lambda_{ex}=325$ nm, $\lambda_{em}=410$ nm). Computer fits were performed using Mathematica (Wolfram, IL) and KaleidaGraph (Synergy Software, PA). The nucleic acid relative fluorescence increase, ΔF_{obs}, upon the polymerase association is defined as $\Delta F_{obs}=(F_i-F_o)/F_o$, where F_i is the fluorescence of the DNA at a given titration point "i", and F_o is the initial fluorescence of the sample [9–11,26,27].

2.5. Quantitative determination of binding isotherms and stoichiometries of the ASFV pol X–ssDNA complexes

In the case of ssDNA oligomers, which accommodate more than one ASFV pol X molecule, quantitative estimates of the total average degree of binding, $\Sigma\Theta_i$, (number of ASFV pol X molecules bound per oligomer) and the free protein concentration, P_F, has been previously described, in detail, by us [28–32].

2.6. Quantitative determination of binding isotherms for the ASFV pol X association with unmodified ssDNAs using the MCT method

Determination of the interaction parameters for the pol X–unmodified nucleic acid complex has been performed using the Macromolecular Competition Titration (MCT) Method [32,33].

2.7. Fluorescence energy transfer measurements

The Förster efficiency of the fluorescence energy transfer, E, from the coumarin donor, located at the 3′ end of the ssDNA oligomer, dT$(pT)_{19}$, to the acceptor, fluorescein moiety, located at the 5′ end of the same oligomer, has been determined using two apparent fluorescence energy transfer efficiencies. The energy transfer efficiency, E_D, obtained from the quenching of the donor fluorescence is defined as [34,35]

$$E_D=\left(\frac{1}{\nu_D}\right)\left(\frac{F_D-F_{DA}}{F_D}\right) \tag{1}$$

where F_D and F_{DA} are the fluorescence of the donor in the absence and presence of the acceptor, respectively, ν_D is the fraction of the donor in the complex with the acceptor [36]. In the case of the complex with the ASFV pol X, F_D and F_{DA} include the protein effect on the donor emission.

The apparent fluorescence transfer efficiency, E_A, has been determined, using the sensitized acceptor fluorescence, by measuring the fluorescence intensity of the acceptor (fluorescein at the 5' end of the ssDNA oligomer), excited at a wavelength where a donor (coumarin at the 3' end of the ssDNA oligomer) predominantly absorbs, in the absence and presence of the donor. The fluorescence intensities of the acceptor in the absence, F_A, and presence, F_{AD}, of the donor are defined as [34,35]

$$F_A=I_o\varepsilon_A C_{AT}\phi_F^A \tag{2a}$$

and

$$F_{AD}=(1-\nu_A)F_A+I_o\varepsilon_A\nu_A C_{AT}\phi_B^A+I_o\varepsilon_D C_{DT}\nu_D\phi_B^A E_A \tag{2b}$$

where I_o is the intensity of incident light, C_{AT} and C_{DT} are the total concentrations of the acceptor and the donor, ν_A is the fraction of acceptors in the complex with donors, ε_A and ε_D are the molar absorption coefficients of the acceptor and the donor at the excitation wavelength, respectively, ϕ_F^A and ϕ_B^A are the quantum yields of the free acceptor and the acceptor in the presence of the donor. All quantities in Eqs. (2a) and (2b) can be experimentally determined. In the case of the complex with the ASFV pol X, the values of, ϕ_F^A and ϕ_B^A have been obtained by exciting the acceptor in its absorption band where there is no donor absorption to determine any protein effect on the observed ratio of the acceptor quantum yield. Dividing Eqs. (2a) by (2b) and rearranging provides E_A, as

$$E_A=\left[\frac{1}{\nu_D}\right]\left(\frac{\varepsilon_A C_{AT}}{\varepsilon_D C_{DT}}\right)\left\{\left(\frac{\phi_F^A}{\phi_B^A}\right)\left[\left(\frac{F_{AD}}{F_A}\right)+\nu_A-1\right]-\nu_A\right\} \tag{3}$$

The Förster energy transfer efficiency, E, is related to E_D and E_A, by [27,34,35]

$$E=\frac{E_A}{(1-E_D+E_A)} \tag{4}$$

The fluorescence energy transfer efficiency between the donor and the acceptor dipoles, E, is related to the average distance, R, separating the dipoles by [24–37]

$$R=R_o\left[\frac{(1-E)}{E}\right]^{\frac{1}{6}} \tag{5}$$

where, $R_o=9790(\kappa^2 n^{-4}\phi_d J)^{1/6}$, is the so called Förster critical distance (in angstroms), the distance at which the transfer efficiency is 50%, κ^2 is the orientation factor, ϕ_d is the donor quantum yield in the absence of the acceptor, and n is the refractive index of the medium ($n=1.4$), the overlap integral, J, characterizes the resonance between the donor and acceptor dipoles. The Förster critical distance, $R_o=52$ Å, for fluorescein and coumarin, attached to the 5′ and 3′ end of $dT(pT)_{19}$, respectively, has been previously determined by us [34–36].

3. Results

3.1. The DNA-binding subsites within the total DNA-binding site of the ASFV pol X–ssDNA complexes

As mentioned above, the difference between the numbers of ions released exclusively from the strong ssDNA-binding subsite, as compared to the total DNA-binding site of the ASFV pol X, upon binding to the ssDNA, indicates that at [NaCl] lower than ~100 mM the heterogeneity of the total DNA-binding subsite should be strongly diminished, or cease to exist [9]. In other words, if the ion releases are events localized at a particular subsite within the total site and the subsites are independent, at lower salt concentrations, both subsites should have a similar capability of engaging the ssDNA [9]. In such case, the observed transition from the exclusive engagement of the strong subsite of the enzyme in interactions with the nucleic acid to the engagement of the total binding site in interactions with the DNA and reflected in the nonlinear dependence of the macroscopic binding constant as a function of the ssDNA length, would not be observed [9]. Therefore, to address the issue of the engagement of the different DNA-binding subsites of the ASFV pol X, in interactions with the ssDNA, we examined binding of the enzyme to the ssDNA oligomers, differing in the numbers of nucleotides [9,10,31].

Fluorescence titrations of the selected set of ssDNA oligomers, 8-, 10-, 16-, 18-, and 20-mer, $d\varepsilon A(p\varepsilon A)_7$, $d\varepsilon A(p\varepsilon A)_9$, $d\varepsilon A(p\varepsilon A)_{15}$, $d\varepsilon A(p\varepsilon A)_{17}$, and $d\varepsilon A(p\varepsilon A)_{19}$, with the ASFV pol X in buffer C, are shown in Fig. 2a. A single ASFV pol X molecule binds to all examined oligomers [9]. Binding

of the enzyme to the etheno-derivatives of the ssDNA induces a strong increase of the nucleic acid fluorescence, indicating a significant change in the structure of the bound DNA [9]. Moreover, the midpoint of the titration curves shifts toward the lower [ASFV pol X] for the longer nucleic acids, indicating an increased macroscopic affinity of the polymerase for the longer oligomers [9]. The titration curves in Fig. 2a have been analyzed using the single site-binding isotherm defined as

$$\Delta F = \Delta F_{max}\left[\frac{K_N P_F}{1 + K_N P_F}\right] \quad (6)$$

where K_N is the macroscopic binding constant characterizing the affinity for a given ssDNA oligomer, containing N nucleotides. The solid lines in Fig. 2a are nonlinear least-squares fits of the experimental titration curves to Eq. (6) with K_N and ΔF_{max} as fitting parameters.

The dependence of the macroscopic binding constant, K_N, for the ASFV pol X binding to all examined ssDNA oligomers, upon the length of the ssDNA oligomer, is shown in Fig. 2b. In spite of the fact that at the examined salt concentration, the affinity difference between the strong and the weak DNA-binding subsite should be minimal, if any (see above), the plot shows an unusual nonlinear behavior [9]. It is built of two linear parts separated by an intermediate region as

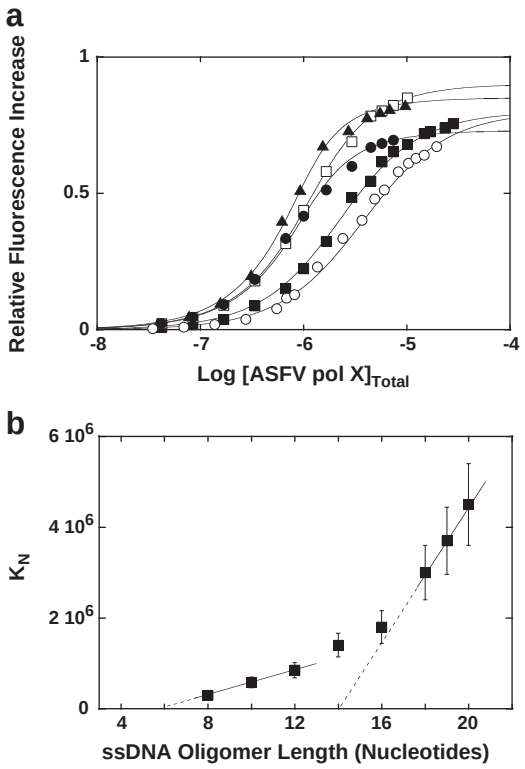

Fig. 2. a. Fluorescence titrations of 8-, 10-, 16-, 18-, and 20-mer, dεA(pεA)$_7$, dεA(pεA)$_9$, dεA(pεA)$_{15}$, dεA(pεA)$_{17}$, and dεA(pεA)$_{19}$ ($\lambda_{ex}=325$ nm, $\lambda_{em}=410$ nm) with the ASFV pol X, in buffer C (pH 7.0, 10 °C), containing 50 mM NaCl and 1 mM $MgCl_2$. Concentrations of all ssDNA oligomers are 1×10^{-6} M. (○) $K=3.0\times10^5\ M^{-1}$, $\Delta F_{max}=0.8$; (■) $K=5.8\times10^5\ M^{-1}$, $\Delta F_{max}=0.8$; (●) $K=1.8\times10^6\ M^{-1}$, $\Delta F_{max}=0.9$; (❑) $K=3.0\times10^6\ M^{-1}$, $\Delta F_{max}=0.73$; (▲) $K=4.3\times10^6\ M^{-1}$, $\Delta F_{max}=0.85$. The solid lines are nonlinear least-squares fits using the single-site binding isotherm (Eq. (6)). b. The dependence of the macroscopic binding constant K_N, upon the length of the ssDNA. The solid line for the part of the plot corresponding to oligomers from 8 to 12 nucleotides is a linear least-squares fit to Eq. (8). Extrapolation of the line to $K_N=0$ intercepts the DNA length axis at $N_p=6.0\pm1.0$. The solid line for the part of the plot corresponding to oligomers from 18 to 20 nucleotides is a linear least-squares fit to Eq. (10). Extrapolation of the line intercepts the DNA length axis at $N_q=14.0\pm1.0$ (details in text).

observed in conditions where the affinities between the strong DNA-binding subsite and the total DNA-binding site were significant [9]. The simplest explanation of the linear part of the K_N plot as a function of the length of the ssDNA oligomers, for the oligomers from 8 to 12 nucleotides in length, is that there is a small, discrete binding region within the total DNA-binding site of the ASFV pol X, characterized by the strong nucleic acid affinity, that experiences the presence of several potential binding sites on the ssDNA oligomers [9,38–41]. This strong DNA-binding subsite engages in interactions a number, p, of nucleotides. Therefore, the values of K_N contain a statistical factor that can be analytically defined in terms of, p, and the intrinsic binding constant, K_p, as [9,38–42]

$$K_N = (N-p+1)K_p \quad (7)$$

and

$$K_N = NK_p-(p+1)\ K_p \quad (8)$$

Extrapolation of the initial linear part of the plot in Fig. 2b, for the oligomers from 8 to 12 nucleotides, to the zero value of the macroscopic equilibrium constant, K_N, intercepts the abscissa at the DNA length, N_p, corresponding to the length of the ssDNA oligomer, which is too short to form a complex with the strong DNA-binding subsite of the enzyme. Introducing $K_N=0$ into Eq. (8) provides the value of N_p as

$$N_p = p-1 \quad (9)$$

The plot in Fig. 2b gives $N_p=6\pm1$. Therefore, in the examined solution conditions, the strong DNA-binding subsite preserves its dominance in the intrinsic affinity of the enzyme and engages in interactions, $p=7\pm1$ nucleotides of the ssDNA [9,38–41]. The intrinsic binding constant, K_p, is determined by the slope of the linear region in Fig. 2b (Eq. (8)), which provides the value of $(1.4\pm0.4)\times10^5\ M^{-1}$ (see Discussion).

For the ssDNA oligomers exceeding 12 nucleotides in length, the plot in Fig. 2b becomes nonlinear and passes through an intermediate region, for the oligomers containing 14 and 16 nucleotides, into the second linear part for the oligomers with the length exceeding ~16 nucleotides [9,31]. The transition between two linear regions of the plot of the macroscopic binding constant as a function of the length of the ssDNA oligomers indicates that an additional DNA-binding subsite, characterized by a different intrinsic affinity, becomes involved in interactions with the nucleic acid. Thus, the enzyme engages its total DNA-binding site, built of a minimum two different DNA-binding subsites, in interactions with the longer ssDNA oligomers [9,31]. The second linear part of the plot in Fig. 2b can be described by expressions analogous to Eqs. (7) and (8), as

$$K_N = NK_q-(q+1)K_q \quad (10)$$

and

$$N_q = q-1 \quad (11)$$

The quantity, q, is the length of the ssDNA oligomer that directly interacts with the total DNA-binding site of the polymerase and K_q is the intrinsic binding constant for the total DNA-binding site. Extrapolation of this region to the $K_N=0$ provides $N_q=14.1\pm1.0$ and $q=15.1\pm1.0$. Thus, the total DNA-binding site of the ASFV pol X engages in direct interactions with the DNA ~15 nucleotides. Notice, this value is lower than the site-size of the total DNA-binding site of the enzyme, which is $n=16\pm1$ nucleotides and remains unaffected by the lower salt concentration (data not shown) [9,31]. The slope of the linear region, for the ssDNA oligomers with the length between 18

and 20 nucleotides, provides $K_q = (7.5 \pm 2.1) \times 10^5\ M^{-1}$ (see Discussion).

3.2. Location of the strong-ssDNA-binding subsite on the ASFV pol X. Macromolecular Competition Titrations Method (MCT)

Previous FRET data showed that the dsDNA 10-mer binds to the C-terminal domain, indicating that the strong DNA-binding subsite is located on the C-terminal domain (Fig. 1a and b) [10]. To unequivocally determine that the same strong DNA-binding subsite is functional in the case of the ssDNA, we performed direct competition studies between the dsDNA 10-mer and the ssDNA 10-mer, using the MCT method (Materials and Methods) [32,33]. Fluorescence titrations of the ssDNA 10-mer, dεA(pεA)$_9$, with the ASFV pol X, in the presence of the unmodified dsDNA 10-mer, is shown in Fig. 3. For comparison, the titration of dεA(pεA)$_9$ alone is also included. A large shift of the titration curve in the presence of the dsDNA indicates very efficient competition between the ssDNA and the dsDNA for the same, *i.e.*, the strong-DNA-binding subsite of the enzyme. In other words, the strong DNA-binding subsite on the C-terminal domain is functional in both the ss and the dsDNA-binding processes.

The interacting system is composed of two short ssDNA lattices competing for the ASFV pol X. The partition functions, Z_{S10} and Z_{D10}, for the ssDNA and dsDNA 10-mer, respectively, are

$$Z_{S10} = 1 + K_{S10} P_F \tag{12}$$

and

$$Z_{D10} = 1 + K_{D10} P_F \tag{13}$$

where K_{S10} and K_{D10}, are the macroscopic binding constants for the ASFV pol X binding to the ssDNA and the dsDNA 10-mer, respectively. The concentration of the bound protein, P_b, is then

$$P_b = \left[\frac{K_{S10} P_F}{1 + K_{S10} P_F}\right] N_{TR} + \left[\frac{K_{D10} P_F}{1 + K_{D10} P_F}\right] N_{TS} \tag{14}$$

or

$$P_b = (\Sigma\Theta_i)_S N_{TR} + (\Sigma\Theta_i)_D N_{TS} \tag{15}$$

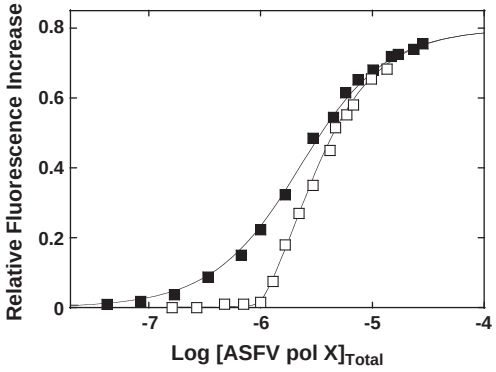

Fig. 3. Fluorescence titrations ($\lambda_{ex} = 325$ nm, $\lambda_{em} = 410$ nm) of the ssDNA 10-mer, dεA(pεA)$_9$, with ASFV pol X in buffer C (pH 7.0, 10 °C), containing 50 mM NaCl and 1 mM $MgCl_2$, in the absence (■) and presence (❑) of the dsDNA 10-mer. The concentrations of the nucleic acids are 1.0×10^{-6} M and 3.0×10^{-6} M, respectively. The solid lines are nonlinear least-squares fits of the fluorescence titration curves, using Eqs. (12)–(16) with the binding constant for dεA(pεA)$_9$, $K_{18} = 5.8 \times 10^5\ M^{-1}$ and $\Delta F_{max} = 0.8$, and the intrinsic binding constant $K_{10S} = 3 \times 10^8\ M^{-1}$ for the unmodified dsDNA 10-mer (details in text).

and

$$P_F = P_T - P_b \tag{16}$$

where P_T is the total concentration of the ASFV pol X, $(\Sigma\Theta_i)_S$ and $(\Sigma\Theta_i)_D$, are the total average degrees of binding of the ASFV pol X on the ss and the dsDNA oligomer, respectively, N_{TR} and N_{TS} are the total concentrations of the fluorescent ssDNA and the unmodified dsDNA 10-mer, respectively. The solid lines in Fig. 3 are nonlinear least-squares fits of the experimental titration curves, with a single fitting parameter, K_{D10}, using Eqs. (12)–(16) and $K_{S10} = 5.8 \times 10^5\ M^{-1}$, and $\Delta F_{max} = 0.8$, independently determined for dεA(pεA)$_9$. The obtained binding constant for the dsDNA 10-mer is, $K_{D10} = (3.0 \pm 0.9) \times 10^8\ M^{-1}$, in excellent agreement with the previously determined value, in analogous solution conditions [10].

3.3. Engagement of the DNA-binding subsite on the N-terminal domain of the ASFV Pol X in interactions with the ssDNA

Once the strong ssDNA-binding subsite on the C-terminal domain has associated with the nucleic acid, the engagement of the DNA-binding subsite on the N-terminal domain, in complexes with the ssDNAs, encompassing the total DNA-binding site, would require strong bending of the nucleic acid, due to structural constraints of the small enzyme molecule (Fig. 1a and b). Such DNA bending is then direct and strong evidence that an efficient engagement of the DNA-binding subsite on the N-terminal domain does occur and can be detected using the fluorescence resonance energy transfer (FRET) method [34,35,43–47]. To address the topology of the ASFV pol X–ssDNA complex, we performed FRET measurements of the enzyme complex with the ssDNA 20-mer [34,35].

The applied ssDNA oligomer, dT(pT)$_{19}$, has fluorescein (Fl) at its 5′ end, and the coumarin derivative (CP) at the 3′ end which serve as the fluorescence energy transfer acceptor, and the donor, respectively (Materials and methods) [34,35]. The enzyme affinity for the labeled oligomer is indistinguishable from the affinity determined for the unmodified DNA (data not shown) [9]. The CP moiety has an emission maximum at ~475 nm, which strongly overlaps the fluorescein absorption spectrum, a condition for the FRET to occur [34,35]. Moreover, the values of the limiting anisotropy for the free ssDNA oligomer and its complexes with the enzyme do not exceed ~0.21 (data not shown). This is an indication that the orientation factor, κ^2, does not significantly affect the FRET measurements [35,36].

Fluorescence emission spectra ($\lambda_{ex} = 425$ nm) of the ssDNA 20-mer, dT(pT)$_{19}$-CP-3′, containing only the donor, 5′-Fl-dT(pT)$_{19}$, containing only the acceptor, and 5′-Fl-dT(pT)$_{19}$-CP-3′, containing both the donor and the acceptor, in the absence of the enzyme, are shown in Fig. 4a. The presence of the acceptor induces large quenching of the donor fluorescence, accompanied by an increase of the acceptor fluorescence emission in the presence of the donor. Both features, the donor emission quenching and the sensitized acceptor emission, indicate that an efficient fluorescence energy transfer process occurs [34,35,43,44]. The emission spectrum of the CP donor, in the complex with the Fl acceptor, has been obtained by normalizing the peak of the donor emission spectrum recorded in the absence of the acceptor to the intensity of the donor recorded in the presence of the acceptor. Subsequently, the emission spectrum of the acceptor, in the complex with the donor, has been obtained by subtracting the normalized spectrum of the donor from the spectrum of 5′-Fl-dT(pT)$_{19}$-CP-3′, containing both the donor and the acceptor. The normalized emission spectrum of the CP donor in the presence of the acceptor and the emission spectrum of the acceptor in the presence of the donor are included in Fig. 4a.

Corresponding fluorescence emission spectra of the ssDNA 20-mer, dT(pT)$_{19}$-CP-3′, containing only the donor, 5′-Fl-dT(pT)$_{19}$,

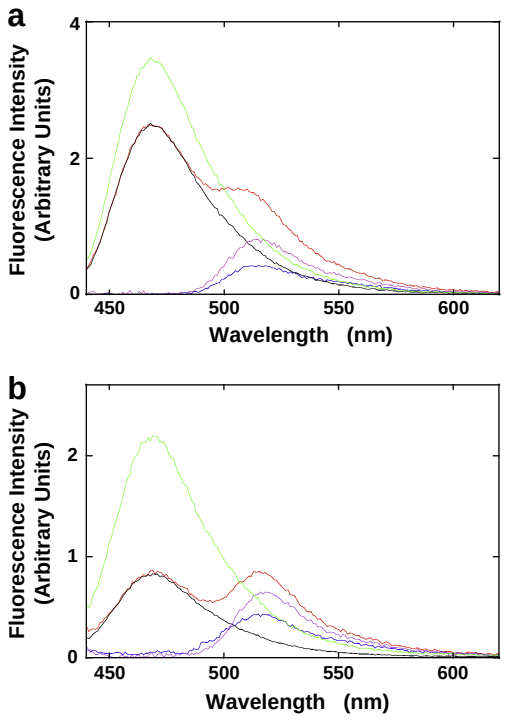

Fig. 4. a. Fluorescence emission spectrum ($\lambda_{ex}=425$ nm) of dT(pT)$_{19}$-CP-3′ (green), 5′-Fl-dT(pT)$_{19}$ (blue), and 5′-Fl-dT(pT)$_{19}$-CP-3′ (red) in buffer C (10 °C) (Materials and methods); the normalized emission spectrum of dT(pT)$_{19}$-CP-3′ to the maximum of CP emission in 5′-Fl-dT(pT)$_{19}$-CP-3′ (black), the sensitized emission spectrum of 5′-Fl-dT(pT)$_{19}$-CP-3′ (magenta). b. Fluorescence emission spectrum, recorded in the presence of the ASFV pol X ($\lambda_{ex}=425$ nm), of dT(pT)$_{19}$-CP-3′ (green), 5′-Fl-dT(pT)$_{19}$ (blue), and 5′-Fl-dT(pT)$_{19}$-CP-3′ (red) in buffer C (10 °C); the normalized emission spectrum of dT(pT)$_{19}$-CP-3′ to the maximum of CP emission in 5′-Fl-dT(pT)$_{19}$-CP-3′ (black), the sensitized emission spectrum of 5′-Fl-dT(pT)$_{19}$-CP-3′ (magenta). Concentrations of the ssDNA oligomers and the ASFV pol X are: 5×10^{-8} M (oligomer) and 5×10^{-6} M.

containing only the acceptor, and 5′-Fl-dT(pT)$_{19}$-CP-3′, containing both the donor and the acceptor, saturated with the ASFV pol X, are shown in Fig. 4b. Both the quenching of the donor fluorescence and the increase of the acceptor fluorescence emission are significantly more pronounced in the presence of the enzyme, than observed for the ssDNA oligomer alone, indicating a strong increase of the fluorescence energy transfer efficiency in the examined ASFV pol X–ssDNA 20-mer system. Analysis of the spectra has been performed as described above (Fig. 4a). The normalized emission spectrum of the donor in the presence of the acceptor and the emission spectrum of the acceptor in the presence of the donor, in the 20-mer–ASFV pol X complex is included in Fig. 4b.

The apparent fluorescence energy transfer efficiencies, E_D and E_A, Förster fluorescence energy transfer efficiency, E, and the average distance between the donor and acceptor, R, have then been calculated using Eqs. (8)–(12)[34,35]. In the absence of the enzyme, $E_D=0.28\pm0.03$ and $E_A=0.48\pm0.05$, $E=0.40\pm0.05$, and $R=55.6\pm3$ Å. The value of R is shorter than the distance (~70 Å) between the 5′ and 3′ end of the nucleic acid in the dsDNA B structure, indicating that dT(pT)$_{19}$ is folded in solution, reflecting the low persistence length of the oligomer. On the other hand, in the presence of the polymerase, $E_D=0.62\pm0.03$ and $E_A=1.00\pm0.05$, $E=0.76\pm0.05$, and $R=42.9\pm3$ Å. These much larger values of the FRET efficiencies and the value of the distance between the acceptor at the 5′ end of the oligomer and the donor, at the 3′ end of the nucleic acid, which is ~13 Å shorter than that determined for the free ssDNA oligomer, strongly indicate that the nucleic acid is profoundly bent in the complex with the ASFV pol X (see Discussion).

3.4. Temperature effect on the ssDNA binding to the strong DNA-binding subsite and to the total DNA-binding site of the ASFV Pol X

The energetics of the ssDNA binding to the strong DNA-binding subsite and the total DNA-binding site of the ASFV pol X have been further addressed by examining the temperature effect on the enzyme binding to the ssDNA oligomers, which exclusively associates with the strong DNA-subsite, or encompass the total DNA-binding site. Fluorescence titrations of dεA(pεA)$_9$ with the ASFV pol X, performed at different temperatures, are shown in Fig. 5a. Titrations of the 18-mer, dεA(pεA)$_{17}$, which encompasses the total DNA-binding site of the enzyme, are shown in Fig. 5b. In both cases, as the temperature increases, the titration curves shift toward lower protein concentrations, indicating an increased macroscopic affinity. Moreover, the values of ΔF_{max} are also increased at higher temperatures, indicating a change in the structure of the bound DNAs. The solid lines in Fig. 5a and b are nonlinear least-squares fits of the titration curves (Eq. (6)), with K_N and ΔF_{max} as fitting parameters.

Fig. 5c shows the dependence of the natural logarithm of the binding constant, K_N, upon the reciprocal of the temperature (Kelvin) (van't Hoff plot) for the selected set of ssDNA oligomers [48]. Within experimental accuracy, the plots are linear. The characteristic features of the plots are that the absolute values of the negative slopes increase with the length of the ssDNA. The slopes of the plots are related to the apparent enthalpy of the binding process by

$$\frac{d\mathrm{Ln}K_N}{d\left(\frac{1}{T}\right)}=-\frac{\Delta H_N^o}{R}. \quad (17)$$

The obtained values of the apparent enthalpy, ΔH_N^o, for the entire series of the examined ssDNA oligomers are included in Table 1. Using the standard thermodynamic formulas, $\Delta G_N^o=-RT\mathrm{Ln}K_N$ and $\Delta S_N^o=(-\Delta G_N^o+\Delta H_N^o)/T$, one obtains the values of the apparent entropy, ΔS_N^o, of the binding process, which are also included in Table 1. It is evident that the interactions of the ASFV pol X with the ssDNA are characterized by the apparent positive enthalpy changes. Thus, the interactions of the enzyme, exclusively within the strong DNA-binding subsite, as well as within the total DNA-binding site, are completely driven by the apparent positive entropy changes, ΔS_N^o (see Discussion).

The dependence of ΔH_N^o upon the length of the ssDNA oligomers is shown in Fig. 6a. The analogous plot for ΔS_N^o is shown in Fig. 6b. Both plots have three phases, which are parallel to the three phases of the corresponding macroscopic affinity plot in Fig. 2b. For the oligomers containing 8 to 12 nucleotides, where the enzyme exclusively uses the strong DNA-binding subsite and engages ~7 nucleotides, the values of ΔH_N^o and ΔS_N^o are, within experimental accuracy, the same ~3.1 kcal/mol and ~33 cal/mol deg, respectively. Binding of the oligomers containing 14 and 16 nucleotides, which are in the intermediate plateau region in the affinity plot (Fig. 2b) is characterized by a significantly higher apparent enthalpy and entropy changes with $\Delta H_N^o\approx8.8$ kcal/mol and $\Delta S_N^o\approx59$ cal/mol deg. Finally, binding of 18-, 19-, and 20-mers, which efficiently encompass the total DNA-binding site and engage ~15 nucleotides in direct interactions with the enzyme, is characterized by $\Delta H_N^o\approx14.5$ kcal/mol and $\Delta S_N^o\approx79$ cal/mol deg, independent of the length of the oligomer (see Discussion).

3.5. Association of the ASFV pol X with the ssDNA 24-mer

In order to assess as to what extent the observed thermodynamic characteristics for the ASFV pol X interactions with the ssDNA oligomers, which bind only a single pol X molecule, is reflected in the association with the oligomer that can bind more than one enzyme molecule, we examined the enzyme association with the 24-mer, dεA(pεA)$_{23}$, which can accommodate two ASFV pol X molecules [9]. In a broader sense,

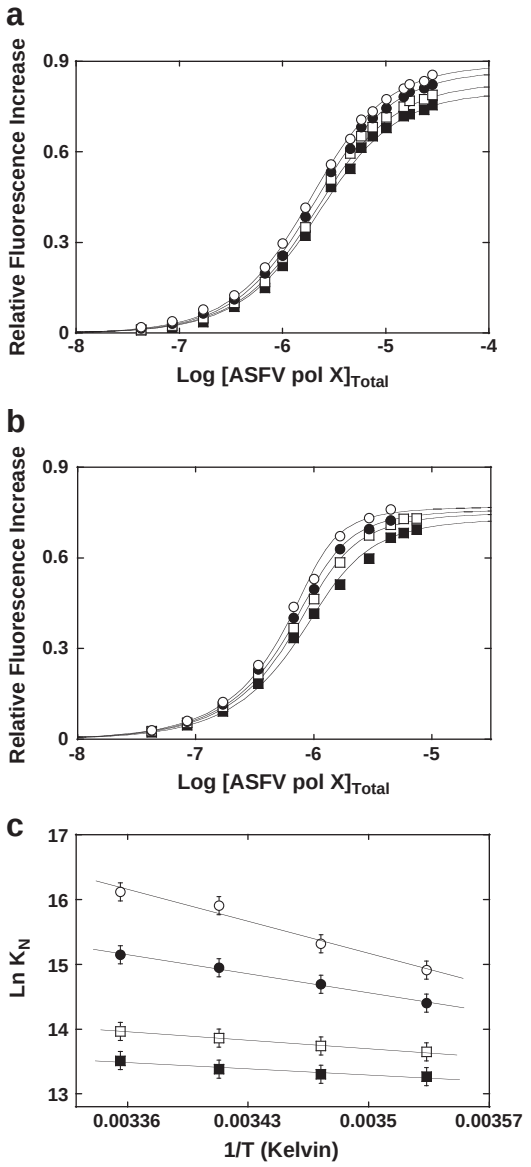

Fig. 5. a. Fluorescence titrations of the ssDNA 10-mer, dεA(pεA)$_9$, with the ASFV pol X ($\lambda_{ex}=325$ nm, $\lambda_{em}=410$ nm) in buffer C (pH 7.0, 10 °C), containing 50 mM NaCl and 1 mM $MgCl_2$, at different temperatures: (■) 10 °C, (❑) 15 °C, (●), 20 °C (○) 25 °C. The concentration of the ssDNA 10-mer is 1×10^{-6} M. The solid line is the nonlinear least-squares fits of the titration curves, using the single-site binding isotherm defined by Eq. (6). b. Fluorescence titrations of the ssDNA 18-mer, dεA(pεA)$_{17}$, with the ASFV pol X ($\lambda_{ex}=325$ nm, $\lambda_{em}=410$ nm) in buffer C (pH 7.0, 10 °C), containing 50 mM NaCl and 1 mM $MgCl_2$, at different temperatures: (■) 10 °C, (❑) 15 °C, (●), 20 °C, (○) 25 °C. The concentration of the ssDNA 18-mer is 1×10^{-6} M. The solid line is the nonlinear least-squares fits of the titration curves, using the single-site binding isotherm defined by eq. (6). c. The dependence of the natural logarithm of the macroscopic binding constants, K_N, upon the reciprocal of the temperature (Kelvin) (van't Hoff plot) for the series of the ssDNA oligomers, differing by the number of the nucleotides. (■) 10-mer dεA(pεA)$_9$, (❑) 12-mer dεA(pεA)$_{11}$, (●) 16-mer dεA(pεA)$_{15}$, and (○) 20-mer dεA (pεA)$_{19}$. The apparent enthalpies and entropies of the examined binding processes are included in Table 1.

these experiments provide information as to what extent the thermodynamic characteristics, observed in complexes with oligomers that accommodate only a single pol X molecule, are reflected in intrinsic binding accompanied by cooperative interactions between bound enzyme molecules on longer nucleic acids. Fluorescence titrations of dεA(pεA)$_{23}$ with the polymerase at two different nucleic acid concentrations, are shown in Fig. 7a. The quantitative determination of the total average degree of binding, $\Sigma\Theta_i$, has been performed using the method outlined in Materials and Methods[9,31–33]. The dependence of ΔF_{obs} as a function of $\Sigma\Theta_i$ of the ASFV pol X on the 24-mer is shown in Fig. 7b. The value of $\Sigma\Theta_i$ could be determined up to ~1.3. Nevertheless, in the examined solution conditions, the plot indicates the presence of two binding phases in the enzyme association with the 24-mer [9].

The simplest statistical thermodynamic model must take into account the fact that the single bound ASFV pol X molecule, associated with the 24-mer, can form two types of complexes engaging $p=7$ or $q=15$ nucleotides, *i.e.*, it can form a complex engaging only the strong DNA-binding subsite or the total DNA-binding site (see above). These two complexes are characterized by different intrinsic binding constants, K_q and K_p, respectively. In the case of the 24-mer, the second bound pol X molecule can only engage its strong DNA-binding subsite, *i.e.*, it occludes only 7 nucleotides [9]. The partition function for the system, Z_{24}, is

$$\begin{aligned} Z_{24} = 1 &+ [(N-q+1)K_q + (N-p+1)K_p]P_F \\ &+ [0.5(N-n-p+1)(N-n-p+2)-(N-n-p+1)]K_qK_pP_F^2 \\ &+ (N-n-p+1)]K_qK_p\omega P_F^2 \end{aligned} \tag{18}$$

where ω is the parameter that characterizes possible cooperative interactions between bound ASFV molecules. The total average degree of binding, $\Sigma\Theta_i$, is then obtained by the standard statistical thermodynamic expression, $\Sigma\Theta_i=\partial\ln Z_{N1}/\partial\ln P_F$, as

$$\Sigma\Theta_i = \frac{\left\{\begin{array}{l}[(N-q+1)K_q + (N-p+1)K_p]P_F \\ \quad + [(N-n-p+1)(N-n-p+2)-2(N-n-p+1)]K_pK_qP_F^2 \\ \quad + [2(N-n-p+1)]K_pK_q\omega P_F^2\end{array}\right\}}{Z_{24}}. \tag{19}$$

The observed relative fluorescence increase of the 24-mer, ΔF, is then

$$\begin{aligned} \Delta F = \Delta F_1\left[\frac{(N-q+1)K_q + (N-p+1)K_p]P_F}{Z_{24}}\right] \\ + \Delta F_{max}\left[\frac{[0.5(N-n-p+1)(N-n-p+2)-(N-n-p+1)]K_pK_qP_F^2}{\quad + [(N-n-p+1)]K_pK_q\omega P_F^2}{Z_{24}}\right] \end{aligned} \tag{20}$$

where ΔF_1 and ΔF_{max} are the relative fluorescence increases accompanying the binding of one and two ASFV pol X molecules to the nucleic acid. The value of ΔF_1 can be determined as the slope of the initial part of the plot in Fig. 7b, $\Delta F_1=\partial\Delta F/\partial(\Sigma\Theta_i)$, leaving K_p, K_q, and ω as fitting parameters. The solid lines in Fig. 7a are nonlinear least-squares fits of the titration curves, using Eqs. (18)–(20). The value of $\omega\approx3.5$ indicates the presence of very weak cooperative interactions between the ASFV pol X molecules associated with the ssDNA [9]. The obtained values of the intrinsic binding constants, $K_p\approx7.0\times10^5$ M^{-1} and $K_q\approx5.5\times10^6$ M^{-1}, are higher by a factor of ~5 - 6 than those obtained with oligomers that can accommodate only a single polymerase molecule, most probably, reflecting a more efficient contact between the protein and the DNA, when the binding sites are embedded within the longer DNA structure [9]. The solid line in Fig. 7b is the computer simulation of ΔF dependence upon $\Sigma\Theta_i$, using the obtained binding parameters, which provide an excellent description of the observed binding process.

Fig. 7c shows the dependence of the natural logarithm of the intrinsic binding constants, K_p and K_q, upon the reciprocal of temperature (Kelvin) (van't Hoff plot) [45]. Within experimental accuracy, the plots are linear. The obtained values of the apparent enthalpy, ΔH^o_p, and ΔH^o_q, are 3.8 ± 0.9 kcal/mol and 11.0 ± 2.1 kcal/mol, respectively. The corresponding apparent entropy changes, ΔS^o_p, and ΔS^o_q, are ~40 cal/mol ° and ~70 cal/mol °, respectively. Thus, these values are very similar to $\Delta H^o_N \approx 3.1$ kcal/mol, and $\Delta S^o_N \approx 33$ cal/mol °, for the ssDNA oligomers that bind a single enzyme molecule and can only engage the strong DNA-binding subsite, and to $\Delta H^o_N \approx 14.5$ kcal/mol, and $\Delta S^o_N \approx 79$ cal/mol °, for the oligomers that engage the total DNA-binding site of the polymerase (see above) (Table 1).

3.6. Solvent effect on the ssDNA binding to the strong DNA-binding subsite and to the total DNA-binding site of the ASFV pol X

To obtain further insight into the ASFV pol X interactions with the ssDNA within the strong DNA-binding subsite and the total DNA-binding site, we examined the solvent effect on the enzyme binding to the ssDNA 10-mer, $d\varepsilon A(p\varepsilon A)_9$, and 18-mer, $d\varepsilon A(p\varepsilon A)_{17}$, respectively. Fluorescence titrations of $d\varepsilon A(p\varepsilon A)_9$ with the ASFV pol X in buffer C (pH 7.0, 10 °C), containing different concentrations of the neutral solute, glycerol (w/v %), are shown in Fig. 8a. Corresponding fluorescence titrations of the 18-mer, $d\varepsilon A(p\varepsilon A)_{17}$, with the polymerase are shown in Fig. 8b. In both cases, at higher [glycerol], the titration curves significantly shift toward lower total protein concentrations, indicating a strong increase of the macroscopic affinity of the protein–nucleic acid complexes. Moreover, the values of ΔF_{max} accompanying the binding greatly increase as the glycerol concentration increases, indicating a significant change of the nucleic acid structure in the complex (see Discussion). To address the question as to what extent the observed dramatic effect of glycerol could be specific for the applied solute, analogous titrations have been performed in the presence of another neutral solute, glucose (data not shown). Similar to the [glycerol] effect, at higher [glucose], the macroscopic affinity of the ASFV pol X - DNA complexes (see Discussion). Analogous behavior was observed in the presence of DMSO, although examined at lower solute concentration (see below). The solid lines in Fig. 8a, and b are nonlinear least-squares fits of the experimental titration curves to Eq. (6) with K_N and ΔF_{max} as fitting parameters.

Though the effect of the "neutral" solute on the macromolecular interactions can be complicated by the presence of preferential interactions, the very similar effect of three different solutes on the same binding process strongly suggests that the preferential interactions do not affect the examined interactions (see below) [49,50]. The simplest thermodynamic model of the observed solute effect is that the association is affected by the changes of the water concentration in the sample [49,50]. The observed equilibrium reaction is then described by a general linkage equation, ASFV pol X + DNA<—>complex + n H_2O.

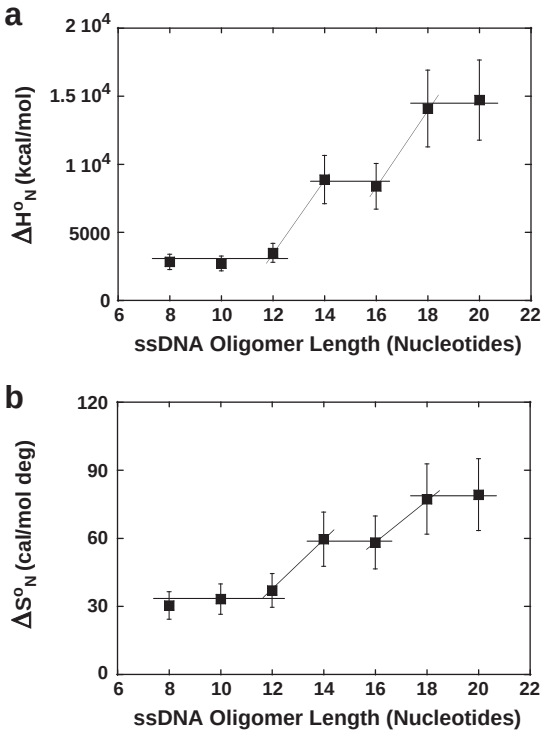

Fig. 6. a. The dependence of the apparent enthalpy, ΔH°, of the ASFV pol X binding to the ssDNA oligomers upon the length of the nucleic acids. b. The dependence of the apparent entropy, ΔS°, of the ASFV pol X binding to the ssDNA oligomers upon the length of the nucleic acids (details in text).

Notice, in the maximum concentration of the applied solutes (*e.g.*, 20% (w/v) glycerol or glucose), the water activity coefficient is practically ~1 [51,52], justifying the use of the water concentration instead of its activity in our studies. In the case of DMSO, at 10% (w/v) concentration of the solute, the water activity coefficient is ~0.97 [53]. The linkage analysis was performed at DMSO concentrations not exceeding 10% (w/v). Moreover, very small effects are completely absorbed by the error in the binding constant determination, which is 15–20% and is included in errors of the determined slopes.

The dependence of the logarithm of the macroscopic binding constants, K_{10} and K_{18} upon the logarithm of $[H_2O]$ (log-log plot), determined in the presence of glycerol, is shown in Fig. 8c [54–58]. Corresponding log-log plots for the enzyme association with the 10- and 18-mer, obtained for the solution containing glucose, are shown in Fig. 8d. The plots are linear in examined solute concentration ranges. In the presence of glycerol, the slopes of the plots are $\partial \log K_{10}/\partial \log[H_2O] = -11.1 \pm 2.1$ and $\partial \log K_{18}/\partial \log[H_2O] = -19.0 \pm 2.5$, respectively. The values of the slopes of the log-log plots, obtained in the

Table 1
Thermodynamic parameters of the binding of the ASFV pol X to the ssDNA oligomers, encompassing the strong DNA-binding subsite and the total DNA-binding site, in buffer C (pH 7.0, 10 °C), containing 1 mM $MgCl_2$ (details in text)[a].

ssDNA Oligomer	Stoichiometry	Site-size	[b]$d\log K_N/d\log[H_2O]$	[c]$d\log K_N/d\log[H_2O]$	[d]$d\log K_N/d\log[H_2O]$	ΔH°kcal/mol	[e]ΔS° cal/mol deg
$d\varepsilon A(p\varepsilon A)_7$	1	7	–	–		2.8 ± 0.7	30 ± 6
$d\varepsilon A(p\varepsilon A)_9$	1	7	−11.1 ± 2.1	−10.9 ± 2.1	−9.9 ± 1.8	2.7 ± 0.6	33 ± 7
$d\varepsilon A(p\varepsilon A)_{11}$	1	7	–	–	–	3.8 ± 0.9	37 ± 8
$d\varepsilon A(p\varepsilon A)_{13}$	1	–	–	–	–	8.9 ± 1.6	60 ± 15
$d\varepsilon A(p\varepsilon A)_{15}$	1	16	–	–	–	8.4 ± 1.6	58 ± 15
$d\varepsilon A(p\varepsilon A)_{17}$	1	16	−19.0 ± 2.5	−17.3 ± 2.3	−18.3 ± 2.3	14.1 ± 2.7	77 ± 19
$d\varepsilon A(p\varepsilon A)_{19}$	1	16	–	–	–	14.7 ± 2.7	79 ± 20

[a] Errors are standard deviations determined using 3–4 independent experiments.
[b] Determined in the presence of glycerol.
[c] Determined in the presence of glucose.
[d] Determined in the presence of DMSO.
[e] Calculated using the intrinsic binding constant obtained at 10 °C.

presence of glucose, are $\partial\log K_{10}/\partial\log[H_2O] = -9.9 \pm 1.8$ and $\partial\log K_{18}/\partial\log[H_2O] = -18.3 \pm 2.3$, respectively (Table 1). Similarly, the values of the slopes of the log-log plots, obtained in the presence of DMSO, are $\partial\log K_{10}/\partial\log[H_2O] = -10.9 \pm 2.1$ and $\partial\log K_{18}/\partial\log[H_2O] = -17.3 \pm 2.3$, respectively (Table 1). First, the values of the slopes of the log-log plots, obtained for three different solutes, are, within experimental accuracy, very similar, indicating that indeed the water concentration is the dominant factor in the observed solute effects. Second, the data indicate that association of the ssDNA oligomer that engages only the strong subsite is accompanied by the net release of ~11 water molecules, while association of the polymerase with the ssDNA, which can engage the total DNA-binding site is accompanied by the net release of ~17–19 water molecules (see Discussion).

4. Discussion

4.1. The two dna-binding subsites of the ASFV Pol X engage sequentially in interactions with the ssDNA

The intricate dependence of the macroscopic binding constant, K_N, upon the length of the ssDNA (Fig. 2b), for the ssDNA oligomers can only occur if the enzyme possesses at least two different intrinsic affinities for the ssDNA [9]. Moreover, these two intrinsic affinities must be generated by at least two interacting areas, which are spatially separated on the enzyme molecule, *i.e.*, two different ssDNA-binding subsites. NMR structure shows the presence of two highly positively charged helices, αC on the N-terminal domain and αE on the C-terminal domain (Fig. 1a and b). The presence of the ssDNA-binding subsite on the N-terminal domain is rather obvious, as it contains the catalytic site of the polymerase [7,8]. However, this is not the subsite with which the polymerase initiates the contact with the nucleic acid [9]. Direct competition experiments using ds and ssDNA 10-mers, described in this work, show that the primary DNA-binding subsite of the ASFV pol X, independent of the DNA conformation, is located on the C-terminal domain [10]. Moreover, FRET data indicate that once the C-terminal domain makes contact with the ssDNA, the enzyme engages the weak DNA-binding subsite on the catalytic N-terminal domain, leading to the strongly bent structure of the bound nucleic acid, as required by the spatial orientation of the DNA-binding subsites (Figs. 1a, b, and 4). The kinetic studies described in the accompanying paper indicate that the engagement of the N-terminal domain is very fast and occurs in a time interval below ~1 ms.

4.2. The intrinsic affinity of the total DNA-binding site is not a simple sum of contributions from the strong and the weak DNA-binding subsites

Although the total site-size of the ASFV pol X - ssDNA complex is 16 ± 1 nucleotides, the enzyme binds only a single molecule of the ssDNA oligomers from 8 to 10 nucleotides in length, even in solution conditions where the intrinsic affinity is strongly amplified by the presence of neutral solutes (see above). These data indicate that the affinity of the weak DNA-binding subsite on the N-terminal domain must be at least ~2 orders of magnitude lower than the affinity of the strong DNA-binding subsite on the C-terminal domain. Otherwise, binding of the second 8- or 10-mer to the enzyme would occur, which is not experimentally observed [9,10]. Surprisingly, the intrinsic binding constants, $K_p \approx 1.4\times10^5\ M^{-1}$ and $K_q \approx 7.5\times10^5\ M^{-1}$, differ only by a factor of ~5. Thus, the weak DNA-binding subsite on the N-terminal domain does make a favorable contribution to the intrinsic affinity of the total DNA-binding site, although not as much as it would be expected from the subsite containing the catalytic site of the polymerase and, which contains the same number of positively charged lysine residues as the strong subsite [9,10].

The data strongly suggest that the ASFV pol X undergoes a significant global conformational change induced by the engagement of the nucleic acid in interactions with the N-terminal domain, accompanied by an unfavorable free energy change, which contributes to the observed large difference in the intrinsic affinities between the two DNA-binding subsites. This conclusion is further supported by the apparent enthalpy changes and previously examined salt effect on the polymerase - ssDNA interactions [9]. While binding of the ssDNA 10-mer is accompanied by a release of ~1.3 ions, interactions of the nucleic acid with the total DNA-binding site lead to the release of ~6 ions. As we pointed out above, this would suggest that the N-terminal domain makes more ionic contacts with the nucleic acid than the C-terminal domain, although both domains contain the same number of three exposed lysine residues [7,8].

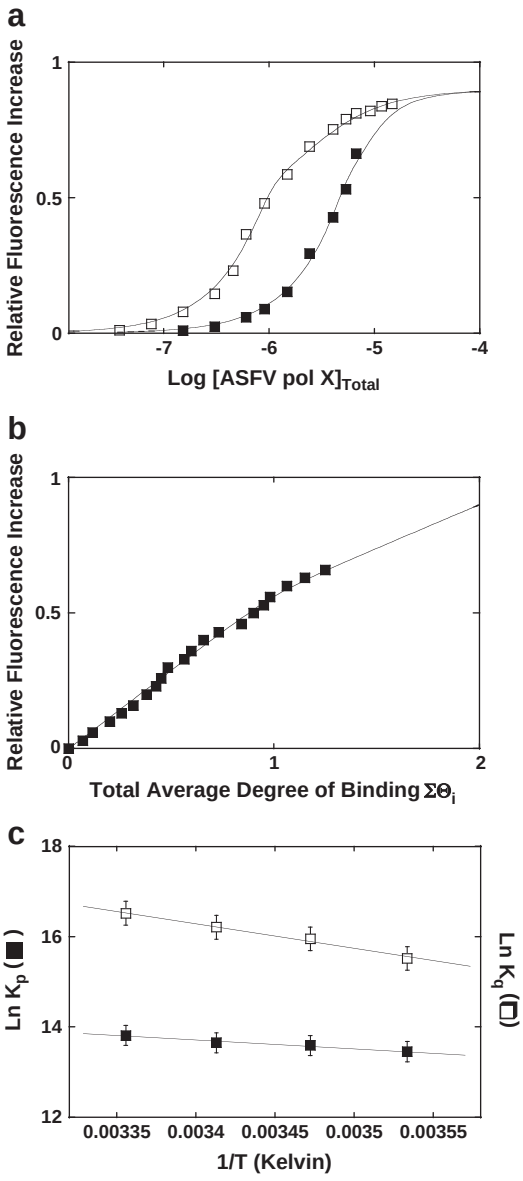

Fig. 7. a. Fluorescence titrations of the ssDNA 24-mer, dεA(pεA)$_{23}$, with the ASFV pol X ($\lambda_{ex} = 325$ nm, $\lambda_{em} = 410$ nm) in buffer C (pH 7.0, 10 °C), containing 50 mM NaCl and 1 mM $MgCl_2$, at two different concentration of the nucleic acid, (□) 1×10^{-6} M and (■) 5.25×10^{-6} M, respectively. The solid lines are nonlinear least-squares fits of the titration curves, using the combinatorial statistical thermodynamic model, described by Eqs. (18)–(20) with $K_q = 5.5\times10^6$ M, $K_p = 7.0\times10^5$ M, $n_q = 16$, $n_p = 7$, $\omega = 1$, $\Delta F_1 = 0.58$, and $\Delta F_{max} = 0.9$ [9]. b. The dependence of the relative fluorescence increase, ΔF_{obs}, upon the total average degree of binding, $\Sigma\Theta_i$, of pol X on the 24-mer. The values of $\Sigma\Theta_i$ have been quantitatively determined using the method described in Materials and methods[31–33]. The solid line is the theoretical dependence of ΔF_{obs} as a function of $\Sigma\Theta_i$, obtained using eqs. 18–20 and obtained binding parameters. c. The dependence of the natural logarithm of the binding constants, K_p (■) and K_q (□), upon the reciprocal of the temperature (Kelvin) (details in text).

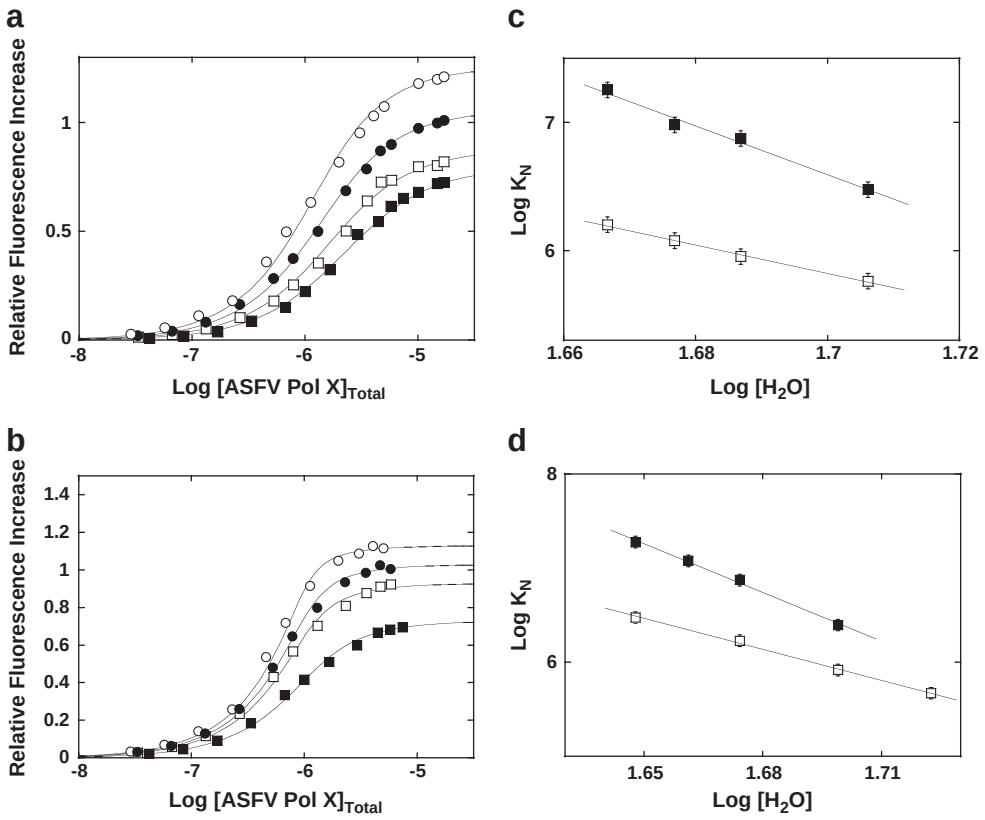

Fig. 8. a. Fluorescence titrations of the ssDNA 10-mer, dεA(pεA)$_9$, with the ASFV pol X ($\lambda_{ex} = 325$ nm, $\lambda_{em} = 410$ nm) in buffer C (pH 7.0, 10 °C), containing 50 mM NaCl, 1 mM $NgCl_2$, and different glycerol concentrations (w/v): 10% (■); 15% (❑); 17.5% (●); 20% (○). **b**. Analogous fluorescence titrations of the ssDNA 18-mer, dεA(pεA)$_{17}$, with the ASFV pol X. The concentration of the ssDNA 10- and the 18-mer is 1×10^{-6} M. The solid lines are nonlinear least-squares fits of the titration curves, using the single-site binding isotherm defined by Eq. (6). b. The dependence of the logarithm of the binding constants, K10 (❑) and K18 (■), upon the logarithm of water concentration. The solid lines are linear least-squares fits, which provide the slopes, $\partial LogK10/\partial Log[H2O] = -11.1 \pm 2.1$ and $\partial LogK19/\partial Log[H2O] = -19 \pm 2.5$, for the 10- and 18-mer, respectively (details in text). d. The dependence of the logarithm of the binding constants, K10 (❑) and K18 (■), upon the logarithm of water concentration determined in the presence of glucose. The solid lines are the linear least-squares fits, which provides the slopes, $\partial LogK10/\partial Log[H2O] = -10.9 \pm 2.1$ and $\partial LogK19/\partial Log[H2O] = -17.3 \pm 2.3$, for the 10- and 18-mer, respectively (details in text).

It also indicates that binding of the nucleic acid to the strong subsite is not dominated by the electrostatic interactions. Notice, the number of ~6 ions released is exactly equal to the number of the lysine residues in the total DNA-binding site, suggesting that, in the final equilibrium complex, all 6 available lysine residues may make contact with the DNA. The observed "asymmetric" ion release strongly suggests that the enzyme adjusts its structure to the nucleic acid associated with the total DNA-binding site, which leads to the engagement of all lysine residues on the C-terminal domain in interactions with the DNA (see below).

4.3. Large positive enthalpy changes accompanying the ASFV pol X–ssDNA interactions indicate that specific conformational changes of complex are induced by the engagement of the DNA-binding subsite on the N-terminal domain of the protein

A striking feature of the ASFV pol X–ssDNA interactions are large and unfavorable enthalpy changes. Moreover the values of the enthalpy changes are dependent upon the length of the associated nucleic acid, *i.e.*, they are very different for the strong DNA-binding subsite, as compared to the total DNA-binding site. Thus, the apparent enthalpy change is ~3–4 kcal/mol for the exclusive association of the strong subsite with the nucleic acid, while interactions of the total DNA-binding site with the DNA is accompanied by $\Delta H^o_N \approx$ ~14–15 kcal/mol (Table 1). These thermodynamic characteristics are preserved in the enzyme complexes with 24-mer indicating that cooperative interactions between bound pol X molecules do not affect the intrinsic interactions with the DNA. Notice, the value of ΔH^o_N could even be larger because the complex, where the total DNA-binding site is associated with the nucleic acid, is in internal equilibrium with the complex where only the strong subsite is engaged in interaction with the DNA [9]. The large difference between the enthalpy changes provides a strong indication that a specific structural transformation of the formed complex does indeed occur upon engagement of the weak DNA-binding subsite (see above).

There are several factors, which could contribute to the observed thermodynamic characteristics. At the excitation wavelength applied ($\lambda_{ex} = 325$ nm), the fluorescence increase of etheno-derivatives of the ssDNA predominantly results from an increase of the quantum yield of the nucleic acid in the complex with the ASFV pol X. Fluorescence of εA is not very sensitive to the polarity of the environment, but is principally affected by the structure of the nucleic acid and reflects the increased separation, *i.e.*, breaking stacking interactions and restricted mobility of the nucleic acid bases [22,23]. The large increase of etheno-derivative fluorescence upon complex formation with the enzyme indicates breaking the stacking interactions and increasing base separation, which must contribute to the observed positive enthalpy change. However, the strong DNA-binding subsite directly engages ~7 nucleotides while the total DNA-binding site directly interacts with ~15 nucleotides. If unstacking of the bases was a predominant cause for the observed positive enthalpy for the engagement of the total binding site, then ΔH^o_N would only be approximately twice as large as that obtained for the strong subsite, *i.e.*, ~6 - 8 kcal/mol, not ~14–15 kcal/mol, as experimentally observed. DNA bending may add to the positive enthalpy change, but the small persistence length of the ssDNA oligomers makes such a contribution, amounting to additional ~7–9 kcal/mol, unlikely.

Notice, binding of the 14- and 16-mer, which make albeit inefficient contact with the N-terminal domain, is characterized by an average value of $\Delta H^{o}_{N} \approx 8.7$ kcal/mol, while an extra two bases, in the case of the 18-mer and full contact with the weak DNA-binding subsite on the N-terminal domain, brings the apparent enthalpy change to the value of ~14 kcal/mol. Moreover, in the case of the 20-mer, a further increase of the oligomer length by two bases, does not significantly affect this value of the apparent enthalpy change (Table 1). The data indicate that the engagement of the N-terminal domain by the bound DNA, which encompasses the total DNA-binding site and the induced global conformational transition of the complex is the major factor responsible for the large positive enthalpy change in the polymerase binding to the ssDNA. In this context, positive but much more modest changes of the apparent enthalpy accompanying the binding of the DNA to the strong DNA-binding subsite on the C-terminal domain could indeed be dominated by the conformational transition of the bound nucleic acid, *i.e.*, breaking of the stacking interactions between bases.

4.4. The intrinsic affinities of the strong DNA-binding subsite and the total DNA-binding site are predominantly driven by large entropy changes resulting from the release of water molecules from both the N-terminal and the C-terminal domain of the enzyme

Unlike the apparent enthalpy changes, the large apparent entropy changes accompanying the DNA binding to the C-terminal or the N-terminal domain correlate well with the length of the associated DNA (Table 1). Thus, direct contact with ~7 nucleotides in the strong DNA-binding site on the C-terminal domain is accompanied by $\Delta S^{o}_{N} \approx$ ~30–40 cal/mol °, while for the engagement of ~15 nucleotides within the total DNA-binding site, is accompanied by $\Delta S^{o}_{N} \approx$ ~80 cal/mol °. Such a "proportional" behavior indicates that both the strong and the weak DNA-binding subsite contribute equally to the observed positive entropy changes. In other words, the apparent entropy changes originate locally at each of the two DNA-binding subsites, without the intervening conformational change of the entire complex. The insight into the nature of the observed apparent entropy change comes from the examination of the solvent effect on the examined intrinsic affinities (Fig. 8c and d, Table 1). Formation of the complex, exclusively at the strong DNA-binding subsite, is accompanied by the release of ~11 water molecules, while binding of the ssDNA oligomer, which encompasses the total DNA-binding site, induces the release of ~19 water molecules, *i.e.*, ~twice as many as the association at the C-terminal domain and resulting in approximately twice as large an entropy change.

The conformational changes of the DNA occurring in the complex, as indicated by the observed fluorescence changes, cannot contribute to the observed positive entropy changes. Strong immobilization of the bases should lead to negative rather than positive entropy changes. Thus, the released water molecules must predominantly originate from the DNA-binding subsites of the polymerase. Interestingly, high glycerol concentrations in solution strongly increase the fluorescence changes accompanying the DNA binding to the enzyme (Fig. 8a). This is in spite of the fact that the solute does not significantly affect the free nucleic acid fluorescence (data not shown). Rather, the increased dehydration of the complex induces further separation and immobilization of the bases of the DNA associated with the enzyme.

The role of the strong DNA-binding subsite on the C-terminal domain emerges as the subsite with high intrinsic affinity that makes primary initial contact with the DNA. Although the physiological role of the weak DNA-binding subsite on the N-terminal domain is defined by the presence of the active site of the polymerase, the role of a very low intrinsic affinity of the weak subsite, resulting from unfavorable enthalpy changes of the formed complex with the nucleic acid, is less clear. It is possible that the low affinity and increased entropy of the weak subsite–DNA complex provide a necessary flexibility of the system for efficient catalysis and required by the constantly changing structure of the associated DNA molecule.

Engagement of the total DNA-binding site is absolutely necessary for catalysis. The large positive apparent enthalpy change characterizing the total DNA-binding site–DNA interactions and the dominant role of water molecules in affecting the intrinsic affinity of the complex indicate that the enzyme can dramatically increase its affinity for the total DNA-binding site at higher temperatures and, particularly, in conditions that mimic the diminished solvent concentration, *e.g.*, by molecular crowding in the cell. Our laboratory is currently addressing these issues.

Acknowledgment

We wish to thank Mrs. Gloria Drennan Bellard for reading the manuscript.

References

[1] R.J. Yanez, J.M. Rodriguez, M.L. Nogal, L. Yuste, C. Enriquez, J.F. Rodriguez, E. Vinuela, Analysis of the complete nucleotide sequence of African swine fever virus, Virology 208 (1995) 249–278.
[2] L.K. Dixon, C.C. Abrams, G. Bowick, L.C. Goatley, P.C. Kay-Jackson, D. Chapman, E. Liverani, R. Nix, R. Silk, F. Zhang, African Swine Fever Virus proteins involved in evading host defense systems, Vet. Immunol. Immunopathol. 100 (2004) 117–134.
[3] N. Jouvnet, T. Wileman, African Swine Fever Virus infection disrupts centrosome assembly and function, J. Gen. Virol. 86 (2005) 589–594.
[4] M. Oliveros, R.R. Yanez, M.L. Salas, J. Salas, E. Vinuela, L. Blanco, Characterization of an African Swine Fever Virus 20-kDa DNA polymerase involved in DNA repair, J. Biol. Chem. 272 (1997) 30899–30910.
[5] R. Garcia-Escudero, M. Garcia-Diaz, M.L. Salas, L. Blanco, J. Salas, DNA polymerase X of African Swine Fever Virus: insertion fidelity on gapped DNA substrates and AP lyase activity support a role in base excision repair of viral DNA, J. Mol. Biol. 326 (2003) 1403–1412.
[6] A.K. Showalter, M.-D. Tsai, A DNA polymerase with specificity for five base pairs, J. Am. Chem. Soc. 123 (2001) 1776–1777.
[7] M. Maciejewski, R. Shin, B. Pan, A. Marintchev, A. Denninger, M.A. Mullen, K. Chen, M.R. Gryk, G.P. Mullen, Solution structure of a viral DNA repair polymerase, Nat. Struct. Biol. 8 (2001) 936–941.
[8] A.K. Showalter, I.-J. Byeon, M.-I. Su, M.-D. Tsai, Solution structure of a viral dna polymerase X and evidence for mutagenic function, Nat. Struct. Biol. 8 (2003) 942–946.
[9] M.J. Jezewska, A. Marcinowicz, A.L. Lucius, W. Bujalowski, DNA polymerase X from African Swine Fever Virus. Quantitative analysis of the enzyme–ssDNA interactions and the functional structure of the complex, J. Mol. Biol. 356 (2006) 121–141.
[10] M.J. Jezewska, P.J. Bujalowski, W. Bujalowski, Interactions of the DNA polymerase X of African Swine Fever Virus with double-stranded DNA. Functional structure of the complex, J. Mol. Biol. 373 (2007) 75–95.
[11] M.J. Jezewska, P.J. Bujalowski, W. Bujalowski, Interactions of the DNA polymerase X from African Swine Fever Virus with gapped DNA substrates. Quantitative analysis of functional structures of the formed complexes, Biochemistry 46 (2007) 12909–12924.
[12] M.T. Washington, W.T. Wolfle, T.S. Spratt, L. Prakash, S. Prakash, Yeast DNA polymerase η makes functional contacts with the DNA minor groove only at the incoming nucleotide triphosphate, Proc. Natl. Acad. Sci. U.S.A. 100 (2003) 5113–5118.
[13] J. Trinacao, R.E. Johnson, W.T. Wolfle, C.R. Escalante, S. Prakash, L. Prakash, A.K. Aggarwal, Dpo4 Is hindered in extending a G.T. mismatch by a reverse wobble, Nat. Struct. Mol. Biol. 11 (2004) 457–462.
[14] J.C. Morales, E.T. Kool, Functional hydrogen-bonding map of the minor groove binding tracks of six DNA polymerases, Biochemistry 39 (2000) 12979–12988.
[15] H. Edelhoch, Spectroscopic determination of tryptophan and tyrosine in proteins, Biochemistry 6 (1967) 1948–1954.
[16] S.C. Gill, P.H. von Hippel, Calculation of protein extinction coefficients from amino acid sequence data, Anal. Biochem. 182 (1989) 319–326.
[17] S. Rajendran, M.J. Jezewska, W. Bujalowski, Human DNA polymerase β recognizes single-stranded DNA using two different binding modes, J. Biol. Chem. 273 (1998) 31021–31031.
[18] M.J. Jezewska, S. Rajendran, W. Bujalowski, Transition between different binding modes in rat DNA polymerase β–ssDNA complexes, J. Mol. Biol. 284 (1998) 1113–1131.
[19] S. Rajendran, M.J. Jezewska, W. Bujalowski, Recognition of template primer and gapped DNA substrates by human DNA polymerase β, J. Mol. Biol. 308 (2001) 477–500.
[20] M.J. Jezewska, S. Rajendran, W. Bujalowski, Energetics and specificity of rat DNA polymerase β interactions with template-primer and gapped DNA substrates, J. Biol. Chem. 276 (2001) 16123–16136.
[21] M.J. Jezewska, S. Rajendran, W. Bujalowski, Interactions of the 8-kDa domain of rat DNA polymerase β with ssDNA, Biochemistry 40 (2001) 3295–3307.

[22] B.M. Baker, J. Vanderkooi, N.R. Kallenbach, Base stacking in a fluorescent dinucleoside monophosphate: εApεA, Biopolymers 17 (1978) 1361–1372.
[23] G.L. Tolman, J.R. Barrio, N.J. Leonard, Chloroacetaldehyde-modified dinucleoside phosphates. Dynamic fluorescence quenching and quenching due to intramolecular complexation, Biochemistry 13 (1974) 4869–4878.
[24] M.J. Jezewska, R. Galletto, W. Bujalowski, Tertiary conformation of the template-primer and gapped DNA substrates in complexes with rat polymerase β. Fluorescence energy transfer studies using the multiple donor–acceptor approach, Biochemistry 42 (2003) 11864–11878.
[25] M.J. Jezewska, S. Rajendran, W. Bujalowski, Interactions of *Escherichia coli* replicative helicase PriA protein with single-stranded DNA, Biochemistry 39 (2000) 10454–10467.
[26] M.J. Jezewska, S. Rajendran, W. Bujalowski, Complex of *Escherichia coli* primary replicative helicase DnaB protein with a replication fork. recognition and structure, Biochemistry 37 (1998) 3116–3136.
[27] M.J. Jezewska, R. Galletto, W. Bujalowski, Interactions of the RepA helicase hexamer of plasmid RSF1010 with the ssDNA. Quantitative analysis of stoichiometries, intrinsic affinities, cooperativities, and heterogeneity of the total ssDNA-binding site, J. Mol. Biol. 343 (2004) 115–136.
[28] T.M. Lohman, W. Bujalowski, Thermodynamic methods for model-independent determination of equilibrium binding isotherms for protein–DNA interactions: spectroscopic approaches to monitor binding, Methods Enzymol. 208 (1991) 258–290.
[29] W. Bujalowski, M.J. Jezewska, Spectrophotometry & spectrofluorimetry, in: M.G. Gore (Ed.), A Practical Approach, Oxford University Press, Oxford, 2000, pp. 141–165.
[30] R. Galletto, M.J. Jezewska, W. Bujalowski, Interactions of the *Escherichia coli* DnaB helicase hexamer with the replication factor the DnaC protein. Effect of nucleotide cofactors and the ssDNA on protein–protein interactions and the topology of the complex, J. Mol. Biol. 329 (2003) 441–465.
[31] W. Bujalowski, M.J. Jezewska, Thermodynamic Analysis of the Structure-Function Relationship in the total DNA-binding site of enzyme–DNA complexes, Methods Enzymol. 466 (2009) 294–324.
[32] W. Bujalowski, Thermodynamic and kinetic methods of analyses of protein–nucleic acid interactions. From simpler to more complex systems, Chem. Rev. 106 (2006) 556–606.
[33] M.J. Jezewska, W. Bujalowski, A general method of analysis of ligand binding to competing macromolecules using the spectroscopic signal originating from a reference macromolecule. Application to *Escherichia coli* replicative helicase DnaB protein–nucleic acid interactions, Biochemistry 35 (1996) 2117–2128.
[34] M.J. Jezewska, S. Rajendran, D. Bujalowska, W. Bujalowski, Does ssDNA pass through the inner channel of the protein hexamer in the complex with the *E. coli* DnaB helicase? Fluorescence energy transfer studies, J. Biol. Chem. 273 (1998) 10515–10529.
[35] M.J. Jezewska, R. Galletto, W. Bujalowski, Tertiary conformation of the template-primer and gapped DNA substrates in complexes with rat polymerase β. Fluorescence energy transfer studies using the multiple donor–acceptor approach, Biochemistry 42 (2003) 11864–11878.
[36] J.R. Lakowicz, Principles of Fluorescence Spectroscopy, Plenum Press, New York, 1999, pp. 367–394.
[37] H.A. Berman, J. Yguerabide, P. Taylor, Fluorescence energy transfer on acethylcholinesterase: Special relationship between peripheral site and active center, Biochemistry 19 (1980) 2226–2235.
[38] J.D. McGhee Test, J. Mol. Biol. 86 (1974) 469–489.
[39] I.R. Epstein, Cooperative and non-cooperative binding of large ligands to a finite one-dimensional lattice. a model for ligand–oligonucleotide interactions, Biophys. Chem. 8 (1978) 327–339.
[40] W. Bujalowski, T.M. Lohman, C.F. Anderson, On the cooperative binding of large ligands to a one-dimensional homogeneous lattice: the generalized three-state lattice model, Biopolymers 28 (1989) 1637–1643.
[41] M.R. Szymanski, M.J. Jezewska, W. Bujalowski, Interactions of the *Escherichia coli* Primosomal PriB Protein with the Single-Stranded DNA. Stoichiometries, Intrinsic Affinities, Cooperativities, and Base Specificities, J. Mol. Biol. 398 (2010) 8–25.
[42] S.A. Latt, H.A. Sober, Protein–nucleic acid interactions. II. oligopeptide-polyribonucleotide binding studies, Biochemistry 10 (1967) 3293–3306.
[43] M. Yang, D.P. Millar, Fluorescence resonance energy transfer as a probe of DNA structure and function, Methods Enzymol. 278 (1997) 417–444.
[44] G. Vamosi, R.M. Clegg, The helix–coil transition of DNA duplexes and hairpins observed by multiple fluorescence parameters, Biochemistry 37 (1998) 14300–14316.
[45] M.A. Trakselis, S.C. Alley, E. Able-Santos, S.J. Benkovic, Creating a dynamic picture of the sliding clamp during T4 DNA polymerase holoenzyme assembly by using fluorescence resonance energy transfer, Proc. Natl. Acad. Sci. U. S. A. 98 (2001) 8368–8375.
[46] L.J. Parkhurst, Distance parameters derived from time-resolved Forster resonance energy transfer measurements and their use in structural interpretations of thermodynamic quantities associated with protein–DNA interactions, Methods Enzymol. 379 (2004) 235–262.
[47] M.F. Bailey, E.H. Thompson, D.P. Millar, Probing DNA polymerase fidelity mechanisms using time-resolved fluorescence anisotropy, Methods 25 (2001) 62–77.
[48] K.A. Connors, Chemical kinetics, The Study of Reaction Rates in Solution, VCH Publishers, New York, 1990, pp. 187–200.
[49] S.N. Timasheff, Protein–solvent interactions, protein hydration, and modulation of biochemical reactions by solvent components, Proc. Natl. Acad. Sci. U. S. A. 99 (2002) 9721–9726.
[50] V.A. Parsegian, R.P. Rand, D.C. Rau, Osmotic stress, crowding, preferential hydration, and binding: a comparison of perspectives, Proc. Natl. Acad. Sci. U. S. A 97 (2000) 3987–3992.
[51] C. Marcolli, Th. Peter, Water activity in polyol/water systems: New UNIFAC parameterization, Atmos Chem. Phys. Discuss. 5 (2005) 1501–1527.
[52] A.M. Sereno, M.D. Hubinger, J.F. Comesana, A. Correa, Prediction of water activity of osmotic solutions, J. Food Eng. 49 (2001) 103–1014.
[53] S.Y. Lam, L. Benoit, Some thermodynamic properties of the dimethylsulfoxide–water and propylene carbonate–water system at 25 °C, Can. J. Chem. 52 (1974) 718–722.
[54] M.T. Record, T.M. Lohman, P.L. deHaseth, Ion effects on ligand–nucleic acid interactions, J. Mol. Biol. 107 (1976) 145–158.
[55] M.T. Record Jr., C.F. Anderson, T.M. Lohman, Thermodynamic analysis of ion effects on the binding and conformational equilibria of proteins and nucleic acids: the roles of ion association or release, screening, and ion effects on water activity, Quart Rev Biophys 11 (1978) 103–178.
[56] M.W. Capp, L.M. Pegram, R.M. Saecker, M. Kratz, D. Riccardi, T. Wendorff, J.G. Cannon, M.T. Record Jr., Interactions of the osmolyte glycine betaine with molecular surfaces in water: thermodynamics, structural interpretation, and prediction of m-values, Biochemistry 43 (2009) 4810372–4810379.
[57] L.M. Pegram, M.T. Record Jr., Quantifying the roles of water and solutes (denaturants, osmolytes, and Hofmeister salts) in protein and model processes using the solute partitioning model, Methods Mol. Biol. 490 (2009) 179–193.
[58] C. Tanford, Extension of the theory of linked functions to incorporate the effects of protein hydration, J. Mol. Biol. 39 (1969) 539–544.